A new uncertainty estimation among multiple datasets and implementation to various precipitation products

Xudong Zhou[1,2], Jan Polcher[2], Tao Yang[1], and Ching-Sheng Huang[1]

[1]State Key Laboratory of Hydrology-Water Resources and Hydraulic Engineering, Center for Global Change and Water Cycle, Hohai University, Nanjing 210098, China
[2]Laboratoire Météorologie Dynamique du CNRS, IPSL, CNRS, Paris, F 91128, France

Abstract.

Ensemble estimates of a certain climatic variable are frequently seen once many parallel datasets are available. Accompanying uncertainties evaluation with the ensemble is recommended while a fundamental flaw is that the uncertainties in temporal variation and spatial heterogeneity are not together considered for the final uncertainty estimate. This study introduces a new three-dimensional variance partitioning approach which avoids pre-averaging in either of the spatio-temporal dimensions. The newly proposed uncertainty estimation (U_e) which integrates the data uncertainties across the spatio-temporal scales is compared with classical uncertainties metrics. Results show that the U_e is around 20% higher than classic metrics for the improvement of uncertainty estimation. The deviation between the metrics is higher for regions with strong spatial heterogeneity and where the temporal variations significantly differ. Decomposing of U_e demonstrates that the new uncertainty estimate is more comprehensive than the classic ones as the components are partially identified by the classic metrics. Multiple precipitation products of different types (gauge-based, merged products and GCMs) are used to better explain and understand the peculiarity of the new methodology. The new uncertainty estimation based on the three-dimensional approach is flexible in its structure and particularly suitable for a comprehensive assessment of multiple datasets over large regions within any given period.

1 Introduction

With the technical development for monitoring the natural climate variables and the increasing knowledge of the physical mechanisms in the climate system, many institutes have the ability to provide different kinds of climate datasets. Taken the precipitation, which is the dominant variable in the land water cycle, as an example, there are point measurements as GHCN-D (global historical climatology network-daily, Menne et al., 2012) , gridded products based on gauge measurements and interpolation (e.g., CRU, Harris et al., 2014) , products derived from remote sensing (e.g., the Tropical Rainfall Measuring Mission -

TRMM), reanalysis datasets (e.g., NCEP) and those estimates from models (e.g., GCMs). These products are developed using different original data, technologies or model settings for various purposes (Phillips and Gleckler, 2006; Tapiador et al., 2012; Beck et al., 2017; Sun et al., 2018). As a result, differences exist among various products due to the measurement errors, model biases or chaotic noises. The uncertainty is thus regarded as the deviation of these model results from the their real values.

5   However, the real values are difficult to measure and uncertainties are difficult to be removed from the datasets. Using ensembles consisting of multiple datasets to generate a weighted average thus becomes very popular in the climate-related researches and the ensemble means are considered as the more reliable estimates. For example, the IPCC uses 42 CMIP5 (Coupled Model Intercomparison Project Phase 5) models to show historical temperature changes and 39 CMIP5 models to average the temperature projection in future RCP 8.5 scenario (Figure SPM.7 in IPCC, 2013b). Schewe et al. (2014) use nine global hydrological

10   models to evaluate the global water scarcity under climate change. GLDAS (Global Land Data Assimilation System) involves four different land surface models (Rodell et al., 2004) and GRACE (Gravity Recovery and Climate Experiment) provides estimations from three independent institutes (Landerer and Swenson, 2012). Using multiple datasets reduces the dependence on a single dataset and eliminate the random variations associated to biases or noises in the model estimates.

     Along with the ensemble means, uncertainty information is recommended to be presented because the uncertainty level

15   decides the reliability of ensemble results. In general, uncertainties can be quantified as the range of maximum and minimum values (i.e., $V_{max} - V_{min}$), range of values at different quantiles (e.g., $V_{5\%} - V_{95\%}$), the consistency of models (ratio of models following a certain pattern to the total number of models), the variation (σ^2) or the standard deviation (σ). These metrics represent different characteristics of the multiple datasets. Among the metrics, the standard deviation (σ) is the most used because it has the same magnitude as the original dataset; it avoids influence of extreme samples and it is less sensitive to the

20   number of datasets used for the investigation. The ratio of the standard deviation (σ) to the mean value (μ), so-called coefficient of variance (CV), representing the dispersion or spread of the distribution of various ensemble members (Everitt, 2013), is a unit-less value which also shows the degree of uncertainty.

     Depending on the purpose of the evaluation, the uncertainty among datasets can be displayed over space to show the spatial heterogeneity of the consistency among multiple datasets . For example, the predicted future temperature increase has a higher

25   significance in the northern high-latitudes among different models than in the middle-latitudes (Box TS.6 Figure 1 in IPCC, 2013a). The other typical implementation is to evaluate the evolution of the model uncertainty over time. In general, the uncertainty range decreases in the historical period over time because more observations are accessible in recent while the range increases for future projections because of the increasing spread of the model simulations (Figure SPM.7 in IPCC, 2013b). The increasing uncertainty range indicates the decreasing of consistency and increasing variations among various

30   datasets.

     The above metrics have been widely used as they show the temporal evolution or spatial distribution of the uncertainty easily. But the short-coming is apparent as only the mean value across one dimension (time or space) is used when we assess the uncertainty for the other dimension (time or space). For example, the averaging over a specific region (spatial mean) is estimated at each time step before the temporal evolution of the model uncertainty can be obtained (red flowcharts in Figure

35   1). And the averaging over a certain period (temporal mean) is estimated at each grid cell before the spatial distribution of the

model uncertainty can be obtained (blue flowcharts in Figure 1). While, the averaging in either dimension means a loss of the information, for instance the data variation. The changes in the variation will not be propagated to the uncertainty estimation if the mean value remains the same. This may result in that the uncertainty among datasets not being fully considered when estimating the uncertainties. In other words, either of the uncertainty estimates cannot represent the full peculiarities among

5   datasets. Therefore, the uncertainty among datasets can be underestimated and the similarity among them overestimated with these two procedures. However current studies have not paid attention to the ignorance of variation due to the averaging as well as its influence on the uncertainty assessment.
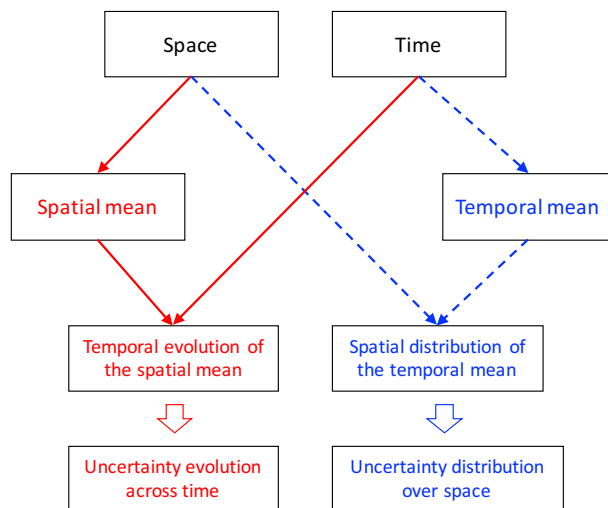
Figure 1. The two classic uncertainty assessments in the current researches as the temporal evolution of the model uncertainty (red) and the spatial distribution of the model uncertainty (blue). Either of the uncertainty estimates has to do the averaging in one of the dimensions in space or time, and it will lead to the loss of information in the corresponding dimension.

The total variation among the multiple datasets is contributed by the uncertainties, temporal variation and the spatial heterogeneity. The key to evaluate the uncertainty is to decompose the variation caused by dataset differences from the others.

10 Though the variation decomposition with method analysis of variance (ANOVA) is often seen in hydro-metrological studies, it is always used to separate the uncertainties generated in series steps that propagated to the final variation. For example, Déqué et al. (2007) separated the uncertainties of regional climate models (RCM) to four sources of uncertainties (sampling uncertainty, model uncertainty, radiative uncertainty and boundary uncertainty), and boundary uncertainty plays a greater role. Bosshard et al. (2013) decomposed the uncertainty in the river streamflow projections to uncertainties from climate models, sta-

15 tistical postprocessing schemes and hydrological models. These implementations differ from the scope of the present study and they fail to separate the uncertainties from the spatio-temporal variations because spatio-temporal averaging has been already applied in the estimation process. Sun et al. (2010, 2012) in the first time decomposed the total variation to temporal variation and spatial heterogeneity. However, it is only valid for the one single dataset and thus not able to evaluate the uncertainties if multiple datasets describe the same variable.

In this study, we aim to introduce a new approach for uncertainty estimation among multiple datasets. The new uncertainty metric avoids any averaging in time or space dimension thus all the information across the two dimensions can be maintained for the uncertainty assessment. Multiple precipitation products are used to explain the peculiarity of the new methodology. In section 2, the detailed methodology of the three-dimensional variance partitioning approach is introduced. The characteristics of multiple precipitation datasets and estimations of the two classic uncertainty metrics are shown in section 3. The results of the new approach for the precipitation products are discussed in section 4. The differences between the new uncertainty estimation and two selected classic metrics introduced previously are analyzed and discussed in section 5. The discussion and conclusions are followed in the end of this article.

2   Methodology and datasets

2.1   Mathematical Derivation

The database consists of multiple datasets that record the same climatic variables in spatio-temporal scale. The database has to be organized in three dimensions of (1) **time** with a regular time interval (e.g. monthly or annual), (2) **space** with regular spatial units where all the grids are re-organized in a new dimension from the original latitude-longitude grids, (3) **ensemble** with different ensemble datasets regarded as the third dimension. Thus, the dataset array can be reformed as

$$\mathbf{Z} = [z_{ijk}] \tag{1}$$

with i-th time step ($i = 1, 2, \ldots, m$), j-th grid ($j = 1, 2, \ldots, n$), and k-th ensemble member or ensemble model ($k = 1, 2, \ldots, l$).

We define the three dimensions as time, space and ensemble dimension and the means for these three dimensions are called temporal mean, spatial mean and ensemble mean, respectively. The corresponding variances are named time variance, space variance and ensemble variance, respectively. The grand mean (μ), grand variance (σ^2) across time, space and ensemble dimensions as well as the total sum of squares (SST) are defined as.

$$\mu = \sum_{i=1}^{m}\sum_{j=1}^{n}\sum_{k=1}^{l} z_{ijk}/(mnl) \tag{2}$$

$$\sigma^2 = \frac{SST}{mnl} \tag{3}$$

$$SST = \sum_{i=1}^{m}\sum_{j=1}^{n}\sum_{k=1}^{l}(z_{ijk} - \mu)^2 \tag{4}$$

The total variation is contributed by the variation in all dimensions (Eq. 4). Thus, it should be reformulated as an express of variations in three different dimensions. The derivation of the total squares can start from the third ensemble dimension. For a

specific k^{th} ensemble member, the grand mean is formulated as $\mu_{ts}[k] = \sum_{i=1}^{m} \sum_{j=1}^{n} z_{ijk}/(mn)$, leading to the total squares rewritten as

$$SST = \sum_{i=1}^{m} \sum_{j=1}^{n} \sum_{k=1}^{l} (z_{ijk} - \mu_{ts}[k] + \mu_{ts}[k] - \mu)^2 \tag{5}$$

The SST can be further expanded and rearranged as

$$SST = \sum_{i=1}^{m} \sum_{j=1}^{n} \sum_{k=1}^{l} (z_{ijk} - \mu_{ts}[k])^2$$

$$+2 \times \sum_{k=1}^{l} (\mu_{ts}[k] - \mu) \underbrace{\left[\sum_{i=1}^{m} \sum_{j=1}^{n} (z_{ijk} - \mu_{ts}[k]) \right]}_{=0}$$

$$+ \underbrace{\left[\sum_{i=1}^{m} \sum_{j=1}^{n} \right]}_{=mn} \sum_{k=1}^{l} (\mu_{ts}[k] - \mu)^2 \tag{6}$$

$$SST = \sum_{i=1}^{m} \sum_{j=1}^{n} \sum_{k=1}^{l} (z_{ijk} - \mu_{ts}[k])^2 + mn \sum_{k=1}^{l} (\mu_{ts}[k] - \mu)^2 \tag{7}$$

$$SST = mn \sum_{k=1}^{l} \sigma_{ts}^2[k] + mnl\sigma^2(\mu_{ts}) \tag{8}$$

Where $\sigma^2(\mu_{ts})$ is the variation of the grand mean for each member of the ensemble, and $\sigma_{ts}^2[k]$, the grand variance in space and time for ensemble member k, can be split using the mean of the spatial variation at each time step $\overline{\sigma_s^2[k,:]}$ and the variation of the spatial mean $\sigma^2(\mu_s[k,:])$, denoted as

$$\sigma_{ts}^2[k] = \overline{\sigma_s^2[k,:]} + \sigma^2(\mu_s[k,:]) \tag{9}$$

The detailed derivation of Eq. (9) is shown in Eqs. (10) - (17). For a specific dataset k, the grand mean $\mu_{ts}[k]$ through space-time scale is

$$\mu_{ts}[k] = \frac{1}{mn} \sum_{i=1}^{m} \sum_{j=1}^{n} z_{ijk} \tag{10}$$

The total square for difference from the grand mean is

$$SST[k] = \sum_{i=1}^{m} \sum_{j=1}^{n} (z_{ijk} - \mu_{ts}[k])^2 \tag{11}$$

and the grand variance σ_{ts}^2 is

$$\sigma_{ts}^2[k] = \frac{1}{mn} \sum_{i=1}^{m} \sum_{j=1}^{n} (z_{ijk} - \mu_{ts}[k])^2 \tag{12}$$

The derivation can start from either the space dimension or the temporal dimension. If starts from the space dimension, Eq. (11) can be rewritten by incorporating the spatial mean of each time step $\mu_s[k,i] = \sum_{j=1}^{l} z_{ijk}/n$

$$SST[k] = \sum_{i=1}^{m}\sum_{j=1}^{n}(z_{ijk} - \mu_s[k,i] + \mu_s[k,i] - \mu_{ts}[k])^2 \tag{13}$$

It can be expanded and then rearranged as

$$
\begin{aligned}
SST[k] =\ & \sum_{i=1}^{m}\sum_{j=1}^{n}(Z_{ijk} - \mu_s[k,i])^2 \\
& + 2 \times \sum_{i=1}^{m}(\mu_s[k,i] - \mu_{ts}[k]) \times \underbrace{\left[\sum_{j=1}^{n}(Z_{ijk} - \mu_s[k,i])\right]}_{=0} \\
& + \underbrace{\left[\sum_{j=1}^{n}\right]}_{=n}\sum_{i=1}^{m}(\mu_s[k,i] - \mu_{ts}[k])^2
\end{aligned}
\tag{14}
$$

$$SST[k] = \sum_{i=1}^{m}\sum_{j=1}^{n}(Z_{ijk} - \mu_s[k,i])^2 + n\sum_{i=1}^{m}(\mu_s[k,i] - \mu_{ts}[k])^2 \tag{15}$$

$$
\begin{aligned}
SST[k] &= n\sum_{i=1}^{m}\sigma_s^2[k,i] + nm\sigma^2(\mu_s[k,:]) \\
&= nm\overline{\sigma_s^2[k,:]} + mn\sigma^2(\mu_s[k,:])
\end{aligned}
\tag{16}
$$

$$\sigma_{ts}^2[k] = \frac{SST[k]}{mn} = \overline{\sigma_s^2[k,:]} + \sigma^2(\mu_s[k,:]) \tag{17}$$

Here $\overline{\sigma_s^2[k,:]}$ is the mean of the spatial variation at each time step and $\sigma^2(\mu_s[k,:])$ is the variation of the spatial mean.

Or if we started from the time dimension, the grand variance can be split using the average of the temporal variation from all regions $\overline{\sigma_t^2[:,k]}$ and the space variation of the temporal mean $\sigma^2(\mu_t[:,k])$:

$$\sigma_{ts}^2[k] = \overline{\sigma_t^2[:,k]} + \sigma^2(\mu_t[:,k]) \tag{18}$$

With Eq. (9) and Eq. (18), we can have

$$\sigma_{ts}^2[k] = \frac{1}{2}\left\{[\sigma^2(\mu_t[:,k]) + \overline{\sigma_s^2[k,:]}] + [\sigma^2(\mu_s[k,:]) + \overline{\sigma_t^2[:,k]}]\right\} \tag{19}$$

Substituting Eq. (19) into Eq. (8) results in

$$
\begin{aligned}
SST =\ & \tfrac{mn}{2}\sum_{k=1}^{l}[\sigma^2(\mu_t[:,k]) + \overline{\sigma_s^2[k,:]}] \\
& + \tfrac{mn}{2}\sum_{k=1}^{l}[\sigma^2(\mu_s[k,:]) + \overline{\sigma_t^2[:,k]}] + mnl\sigma^2(\mu_{ts})
\end{aligned}
\tag{20}
$$

The first term on the right-hand side of Eq. (20) can be transformed to:

$$\frac{mn}{2}\sum_{k=1}^{l}[\sigma^2(\mu_t[:,k]) + \overline{\sigma_s^2[k,:]}] = mnl\left[\overline{\frac{\sigma_{s\_t}^2 + \overline{\sigma_s^2}}{2}}\right] \tag{21}$$

where $\overline{\sigma_{s\_t}^2}$ is the mean of space variation of the temporal mean across each ensemble member, $\overline{\sigma_s^2}$ represents the grand mean of σ_s^2, which is the grand variance across time and ensemble dimensions. Eq. (20) then becomes:

5 $$SST = mnl\left[\overline{\frac{\sigma_{s\_t}^2 + \overline{\sigma_s^2}}{2}}\right] + mnl\left[\overline{\frac{\sigma_{t\_s}^2 + \overline{\sigma_t^2}}{2}}\right] + mnl\sigma_e^2(\mu_{ts}) \tag{22}$$

where $\overline{\sigma_{t\_s}^2}$ is the mean of time variation of the spatial mean across ensembles, $\overline{\sigma_t^2}$ represents the grand mean of σ_t^2, the grand variance across space and ensemble dimensions. $\sigma_e^2(\mu_{ts})$ represents the variation of the spatial-temporal means (μ_{ts}). Similarly, the global derivation of SST can start from any of the other two dimensions. And the SST derived from time and space dimensions are formulated, respectively, as

10 $$SST = mnl\left[\overline{\frac{\sigma_{s\_e}^2 + \overline{\sigma_s^2}}{2}}\right] + mnl\left[\overline{\frac{\sigma_{e\_s}^2 + \overline{\sigma_e^2}}{2}}\right] + mnl\sigma_t^2(\mu_{se}) \tag{23}$$

$$SST = mnl\left[\overline{\frac{\sigma_{e\_t}^2 + \overline{\sigma_e^2}}{2}}\right] + mnl\left[\overline{\frac{\sigma_{t\_e}^2 + \overline{\sigma_t^2}}{2}}\right] + mnl\sigma_s^2(\mu_{et}) \tag{24}$$

Where each variable is defined in the Appendix A. Averaging these three expressions of SST defined in Eqs. (22) - (24) leads to

15 $$\begin{aligned} SST = \quad & \frac{mnl}{3}\left[\frac{\overline{\sigma_{t\_s}^2} + \overline{\sigma_{t\_e}^2}}{2} + \overline{\sigma_t^2} + \sigma_t^2(\mu_{se})\right] \\ & + \frac{mnl}{3}\left[\frac{\overline{\sigma_{s\_t}^2} + \overline{\sigma_{s\_e}^2}}{2} + \overline{\sigma_s^2} + \sigma_s^2(\mu_{et})\right] \\ & + \frac{mnl}{3}\left[\frac{\overline{\sigma_{e\_t}^2} + \overline{\sigma_{e\_s}^2}}{2} + \overline{\sigma_e^2} + \sigma_e^2(\mu_{ts})\right] \end{aligned} \tag{25}$$

With the total degree of freedom ($m \times n \times l$), the grand variance is expressed as

20 $$\begin{aligned} \sigma^2 = \quad & \underbrace{\frac{1}{3}\left[\frac{\overline{\sigma_{t\_s}^2} + \overline{\sigma_{t\_e}^2}}{2} + \overline{\sigma_t^2} + \sigma_t^2(\mu_{se})\right]}_{V_t} \\ & + \underbrace{\frac{1}{3}\left[\frac{\overline{\sigma_{s\_t}^2} + \overline{\sigma_{s\_e}^2}}{2} + \overline{\sigma_s^2} + \sigma_s^2(\mu_{et})\right]}_{V_s} \\ & + \underbrace{\frac{1}{3}\left[\frac{\overline{\sigma_{e\_t}^2} + \overline{\sigma_{e\_s}^2}}{2} + \overline{\sigma_e^2} + \sigma_e^2(\mu_{ts})\right]}_{V_e} \end{aligned} \tag{26}$$

where V_t, V_s and V_e represent the time, space and ensemble variances, respectively. To facilitate the understanding of the partitioning results, an illustration of the present approach is shown in Figure 2.

Note that V_e is estimated based on the combination of variation across the ensemble dimension. The four components are the variations of temporal and spatial values ($\overline{\sigma_e^2}$, zone B3), temporal mean ($\overline{\sigma_{e\_t}^2}$, zone C3), spatial mean ($\overline{\sigma_{e\_s}^2}$, zone C6) and the grand variance of the spatiotemporal mean for a single ensemble member ($\sigma_e^2(\mu_{ts})$, zone F3). Similarly, the other variances only rely on the variances in the corresponding dimension, which shows the independence in the three dimensions.
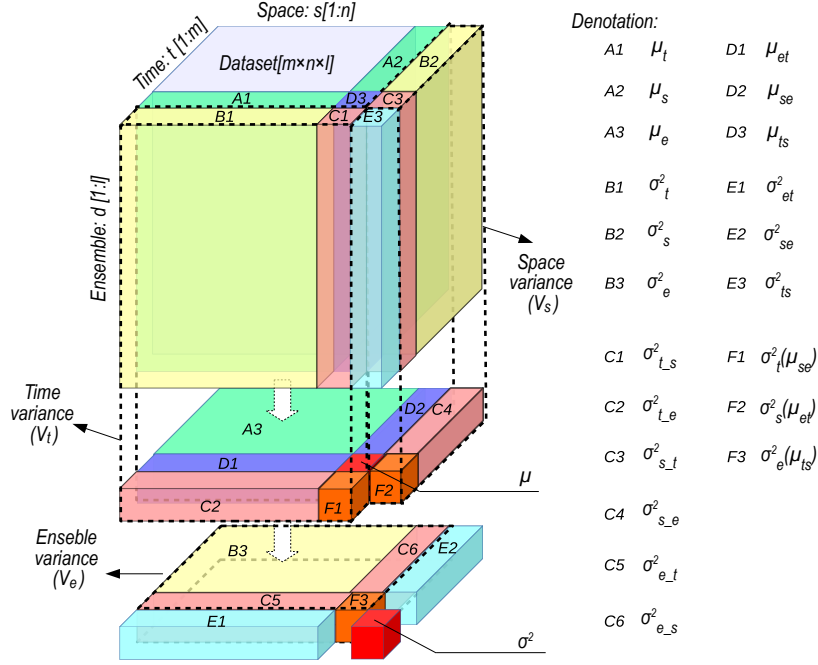
Figure 2. The illustration of the partitioning time-space-ensemble variance method. The original dataset is reorganized into three dimensions of time, space and ensemble. The denotations of the zones are listed to the right. The grand variance is defined as σ^2 and the grand mean as μ. The subscripts t, s, and e represent time, space and ensemble, respectively. Zone A (μ_i) indicates the means of the i dimension; zone B (σ_i^2) indicates the variation for i dimension; zone C ($\sigma_{i\_j}^2$) indicates the variation across i dimension of the means of μ_j; zone D (μ_{ij}) indicates the means across i and j dimensions; zone E (σ_{ij}^2) indicates the variation across i and j dimensions; zone F ($\sigma_i^2(\mu_{jk})$) indicates the variation across i dimension of the means across j and k dimensions. The detailed definitions of these denotations can be found in Appendix A.

5 2.2 Metrics definition for model uncertainty

Since the temporal variation or the spatial heterogeneity is natural in the climate variables and the purpose of this study is to evaluate the model uncertainty among datasets, we focus mainly on the variance in the ensemble dimension. The uncertainty among the ensemble member is normalized as the ratio of the square root of the ensemble variance (V_e) divided by the mean value of the datasets (μ).

10 $$U_e = \sqrt{V_e}/\mu \tag{27}$$

Two classical metrics are also introduced for comparison. For each basic spatial unit (grid cell in this study), we can estimate the long-term mean of the target variable for each dataset $\mu_t[j,k]$, $j = 1,...,n$ represents the space unit, and $k = 1,...,l$ represents the number of datasets. Then for each spatial unit, we can estimate the ensemble variations across different datasets of the mean values as $\sigma^2(\mu_t[j,:])$ (expressed as $\sigma^2_{e\_t}[j]$ in this study). The spatial distribution of the $\sigma^2_{e\_t}$ shows the magnitude of

5 model uncertainty over space and its root $\sigma_{e\_t}[j]$ is the model deviation at each space unit. The overall estimation of the model uncertainty over the entire region can be expressed as:

$$N.s.std = \sqrt{\overline{\sigma^2_{e\_t}}}/\mu = \frac{1}{\mu}\sqrt{\frac{1}{n}\sum_{j=1}^{n}\sigma^2_{e\_t}[j]} \qquad (28)$$

$\sigma^2_{e\_t}[j]$ has different values for each spatial unit and the values for all the grid cells are averaged to obtain $\overline{\sigma^2_{e\_t}}$, which shows the general magnitude of the ensemble variation over space. The $N.s.std$ is normalized as the ratio of the square root of the

10 mean of variations $\sqrt{\overline{\sigma^2_{e\_t}}}$ to the average value of all the datasets μ.

Similarly, the model uncertainty can also be normalized as the ratio of the square root of the averaged ensemble variation at all time steps $\overline{\sigma^2_{e\_s}}$ to the entire means (Eq. 29).

$$N.t.std = \sqrt{\overline{\sigma^2_{e\_s}}}/\mu = \frac{1}{\mu}\sqrt{\frac{1}{m}\sum_{i=1}^{m}\sigma^2_{e\_s}[i]} \qquad (29)$$

where the $\sigma^2_{e\_s}[i], i = 1,...,m$ is the ensemble variation of the spatial mean of each dataset across different datasets of the spatial

15 means of each product at each time unit $\mu_s[i,k], (i = 1,...,m, k = 1,...,l)$. It has different values at different time steps.

The two uncertainty estimates (Eqs. 28 and 29) correspond to the two classic metrics presented in the Introduction. And we will compare the U_e with the two classic metrics ($N.t.std$ and $N.s.std$) to show their relations and percularities.

2.3   Study area and data description

China is large in its area with different climate types encountered in the mainland (Kottek et al., 2006). To facilitate the

20 comparisons and analyses that have spatial variations, ten different subregions are defined in Figure 3 as the (1) Songhua River Basin, (2) Liao River Basin, (3) Hai River Basin, (4) Yellow River Basin, (5) Huai River Basin, (6) Yangtze River Basin, (7) Southeast China, (8) South China, (9) Southwest China, (10) Northwest China. The entire Chinese mainland is numbered as the 11st region. Most of the regions are natural river basins, and this definition is more proper when considering water resources analysis than definitions using longitude-latitude grids or that are based on administrative regions.

25 Thirteen precipitation datasets from different sources are collected for comparison (Table 1). These datasets are categorized into three groups according to the methodologies used to generate the products, i.e., gauge-based products, merged products and General Circulation Models (GCMs). The gauge-based products (i.e., GPCC, CRU, CPC and UDEL) use observed data from global precipitation gauges, while the density of ground observation gauges, the representativeness of the gauges and the interpolation algorithms for converting the gauge observations to gridded dataset vary from product to product. CMA (stands

30 for China Meteorological Administration) dataset uses the densest gauges and probably has the best quality to capture the
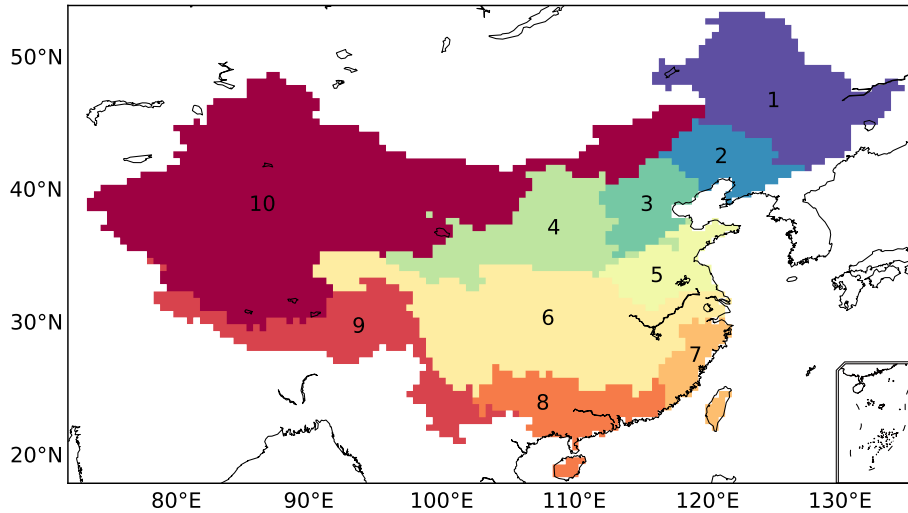
Figure 3. Ten subregions are identified in this study. These subregions are mainly divided as the river basins (regions 1-8) and 9 as the southwestern China and 10 as the northwestern China. The 11 represents the whole mainland.

spatiotemporal variations of the precipitation over the study area. But CMA is excluded when estimating the ensemble means of the gauge-based products and chosen as the reference datasets for comparison.

Among the merged precipitation products, the CMAP, GPCP and MSWEP use different sources of precipitation data (e.g., gauge observations, satellite remote sensing, atmospheric model re-analysis). These different precipitation sources are averaged
5 using different weights. Thus, the differences among the three merged products are associated with the precipitation sources and the weight of the gauge observations. ERA-Interim is a re-analysis product, while it uses near-real-time assimilation with data from global observations (Dee et al., 2011). Thus, the forecasting model is constrained by observations and forced to follow the real system to some degree. Because of the usage of observations, ERA-interim is also belonging to the merged products.
10 GCM precipitation is model estimation, therefore, the physical and numerical choices will affect the accuracy of model results. In addition, observations are not used to constrain the simulations. The lack of constraints on the GCMs will cause them not following the actual synoptic variability and explore other trajectories in the solution space. Kay et al. (2015) repeatedly run the same GCM with a very small difference in the initial conditions, and there is a spread of the model outputs after a number of time steps of running (see Figure 2 in Kay et al., 2015). Therefore, the uncertainty estimated is due to the differences in
15 the model settings and the initial conditions. There are more than 20 datasets of GCMs, while only four are randomly taken to match the number of gauge-based products and merged products.

All the products of three precipitation types including CMA are in gridded format. Though they differ in the spatial resolution, all products are interpolated to $0.5°$ spatial resolution to unify the spatial units. Annual average values are summed up based on their original time steps (daily or monthly) and the overlap time span of all the datasets is selected from 1979 to 2005
20 for the maximum coverage of all products.

Table 1. The precipitation datasets used in this study. Three different precipitation groups are identified according to the way the precipitation dataset is generated.

No	Type	Name	Long name	Institute	Reference
1		CMA	China Meteorological Administration dataset	China Meteorological Administration	
2		GPCC	Global Precipitation Climatology Centre	the World Climate Research Programme (WCRP) and to the Global Climate Observing System (GCOS)	Schneider et al. (2017)
3	Gauge-based	CRU TS	Climatic Research Unit Time-Series	Climatic Research Unit (CRU) / Ian Harris, Phil Jones	Harris et al. (2014)
4		CPC	CPC Global Unified Gauge-Based Analysis of Daily Precipitation	NCEP/Climate Prediction Center	Xie et al. (2007)
5		UDEL	University of Delaware Air Temperature & Precipitation Global (land) precipitation and temperature	University of Delaware	Willmott and Matsuura (2012)
6		CMAP	CPC Merged Analysis of Precipitation	NOAA CPC	Xie et al. (2003)
7	Merged Products	GPCP	Global Precipitation Climatology Project	GSFC (NASA)	Adler et al. (2018)
8		MSWEP	Multi-Source Weighted-Ensemble Precipitation	Princeton University, Princeton, NJ, USA	Beck et al. (2017)
9		ERA-I	ERA-Interim	European Centre for Medium-Range Weather Forecasts	Dee et al. (2011)
10		HadCM3	Hedley Centre Coupled Model Version 3	Met Office Hadley Centre, UK	
11	GCMs	IPSL-CM5A-LR		Insitut Pierre Simon Laplace, Paris, France	
12		CMCC-CM		Cetro Euro-Mediterraneo per I Cambiamenti	
13		MIROC5		AORI, Chiba, Japan, NIES, Ibaraki, Japan, JAMSTEC, Kanagawa, Japan	

3 Characteristics of precipitation and model quantified uncertainties with classic metrics

3.1 Spatial patterns of ensemble annual precipitation

The ensemble means of the long-term annual precipitation (1979-2005) obtained by averaging the multiple datasets in the corresponding precipitation group are mapped in Figure 4. The long-term annual mean precipitation obtained from the CMA data is 589.8 $\mathrm{mm\ yr^{-1}}$ (1.6 $\mathrm{mm\ day^{-1}}$) over mainland China. The gauge-based precipitation has the least bias (-4.1mm $\mathrm{yr^{-1}}$, -0.7% in proportion) compared to the CMA precipitation. Precipitation in the merged products and GCMs is larger than CMA by 63.1 and 232.0 $\mathrm{mm\ yr^{-1}}$ (with the bias as +10.7% and +39.3%), respectively.

The spatial pattern of the annual precipitation shows a decreasing gradient from the southeastern China (>1600 $\mathrm{mm\ yr^{-1}}$) to the northwestern China (<400 $\mathrm{mm\ yr^{-1}}$). All the ensemble means of the three precipitation groups capture the spatial gradient, while they have different ability to express in some details. For instance, some areas have abrupt precipitation changes rather than following the general gradient. This is probably caused by the sudden changes in topography (e.g., the northern Tienshan Mountain, the Qilian Mountains), while it is not captured in the gauge-based products. As we know, the precipitation gauges are mainly distributed on the lower altitude and therefore, they have difficulty in capturing the precipitation events over mountains. The precipitation in the merged products and the GCMs is higher than CMA in Himalayas and particularly the GCMs show higher precipitation in the northern Tibet Plateau as well as the southern part of the Hengduan Mountains. These differences show the general characteristics of the three types of precipitation products.
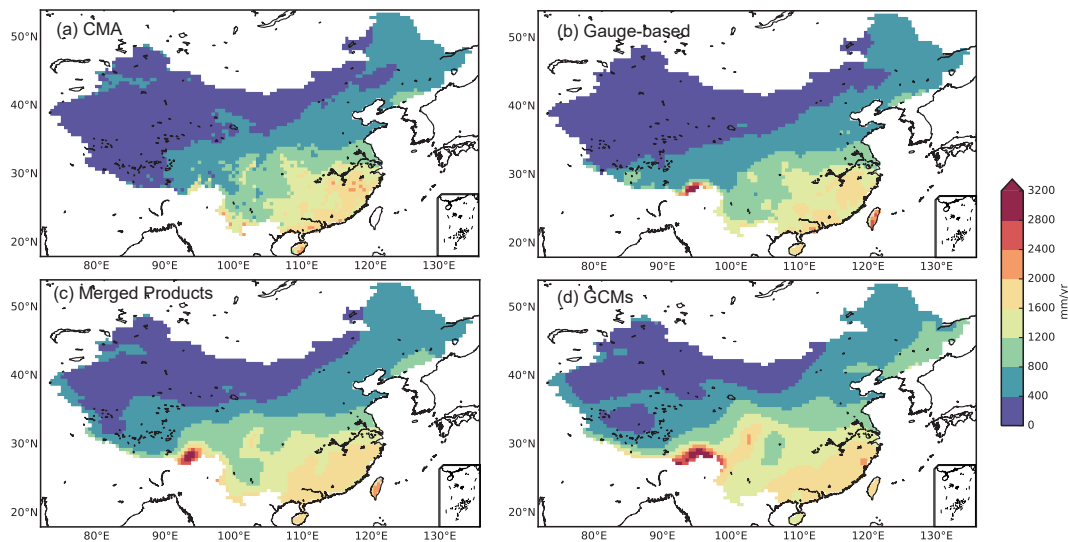
Figure 4. Long-term (1979-2005) annual precipitation in different precipitation groups. (a) Annual precipitation of CMA dataset, (b) ensemble means of the annual precipitation in gauge-based products excluding CMA, (c) ensemble mean of the annual precipitation of all merged products, (d) ensemble means of the annual precipitation of all GCMs. The observations in Taiwan are not included in the CMA dataset.

3.2 Spatial distribution of model uncertainties

In addition to differences of the long-term annual precipitation, differences are found among datasets within the same precipitation group. The spatial distribution of the model uncertainty, which is expressed as the ensemble deviation across multiple products of the annual precipitation, is calculated for each group and mapped in Figure 5.
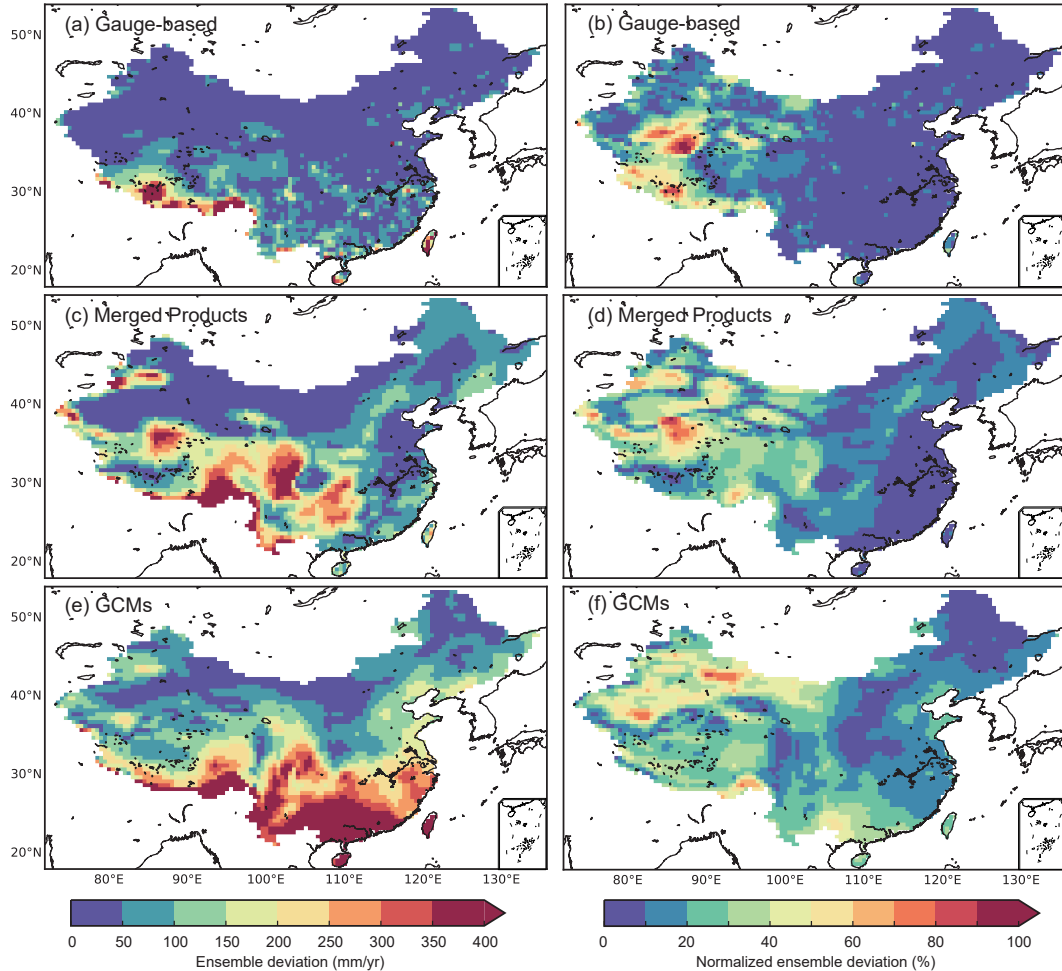
Figure 5. The spatial distribution of the model uncertainty, which is expressed as the ensemble deviation across multiple products of the long-term annual precipitation in each precipitation group (left panels) and the normalized value as the ratio of the ensemble deviation to the ensemble means of the datasets in corresponding group (right panels).

5   Among the datasets based on gauge observations (Figure 5-a), the ensemble deviation value is small in most land area of China (<50 mm yr^{-1}). It is higher in the south of China (50-100 mm yr^{-1}) but the area is not continuous in space. The highest deviation occurs along the Himalayas, indicating a high variation among datasets. Regarding the merged precipitation products, the deviation shows high values (>200 mm yr^{-1}, Figure 5-c) in the southwestern China (e.g., the Tibet Plateau,

Yunnan Province, Guangxi Province). Moderate deviation is found in the northeastern China, northern China and southeastern China. Compared to the gauge-based and merged products, the deviation among GCMs has the highest value (>400 $\mathrm{mm\ yr^{-1}}$, Figure 5-e) in the southern China, indicating a significant model uncertainty of the annual precipitation between different GCMs.

5   The ratio of the ensemble deviation to the mean value, which shows the model uncertainty with no unit, is very low (<10%, Figure 5-b) in the eastern China. While, it is higher in the western China especially in the Himalayas and the northern Tibet Plateau. Similar to that of the gauge-based products, the uncertainty in the merged products has the higher values in the west than that in the east of China (Figure 5-d). The area with the derivation ratio less than 10% is mainly distributed in the southeastern China and is apparently smaller than that of the gauge-based products, showing a decreasing similarity among 10   different merged products. The area with a moderate derivation ratio (10%-40%) increases compared to that of the gauge-based products, and the area is mostly in the middle and western China. The uncertainty estimated in the GCMs shows similar patterns in western China to that of the merged products but with higher magnitudes in the eastern China (Figure 5-f). Only the area in the northeastern and part of the middle China features small uncertainty less than 10%, and the derivation ratio rises significantly in the southern China (e.g., Pearl River basin), which corresponds to the high standard deviation of the GCMs 15   shown in Figure 5-e.

    The magnitude of the ensemble deviation demonstrates the model uncertainty among different precipitation products in the same precipitation group and it shows the ability of the precipitation estimation with different methodologies. For all products, the ensemble deviation is relatively larger where the precipitation is higher, especially along the mountains and the subtropical regions. The derivation ratio is higher in the northwestern China where the precipitation is among the lowest in 20   China. Particularly for the gauge-based products, the higher ratio occurs where the gauge density is low and the orographic effect is apparent (e.g., the Tibet Plateau and the mountainous area). For the merged products and the GCMs, the ratio increases especially in the southeastern China, showing decreasing similarities among different GCMs. Because the ratio has taken into account both the variation and the means (which may have a systematic bias), the derivation ratio is better than the absolute ensemble deviation to represent the uncertainty. Thus it is the most commonly used in the geographic studies.

25   **3.3   Temporal evolution of model uncertainties**

Figure 5 shows the spatial distribution of the ensemble deviation among different precipitation products. However, the temporal evolution of the deviation among the various products is not captured because the temporal variation has been averaged before estimating the ensemble deviation in Figure 5. In this section, we examine the temporal evolution of model uncertainty of the regional annual precipitation across different products. The analysis is based on the ten subregions defined in Figure 3 and the 30   whole Chinese mainland.

    The annual precipitation of each precipitation group has been normalized as the ratio to the long-term annual means of CMA (black line in Figure 6). The magnitude of the annual precipitation in the gauge-based products (the blue curve) is similar to that of CMA except in the southwestern China (Figure 6-i) for the overestimation along the Himalayas (Figure 4). The precipitation in the merged products (the green curve) is higher in the southwestern and northwestern China, in accordance with Figure 4-c.
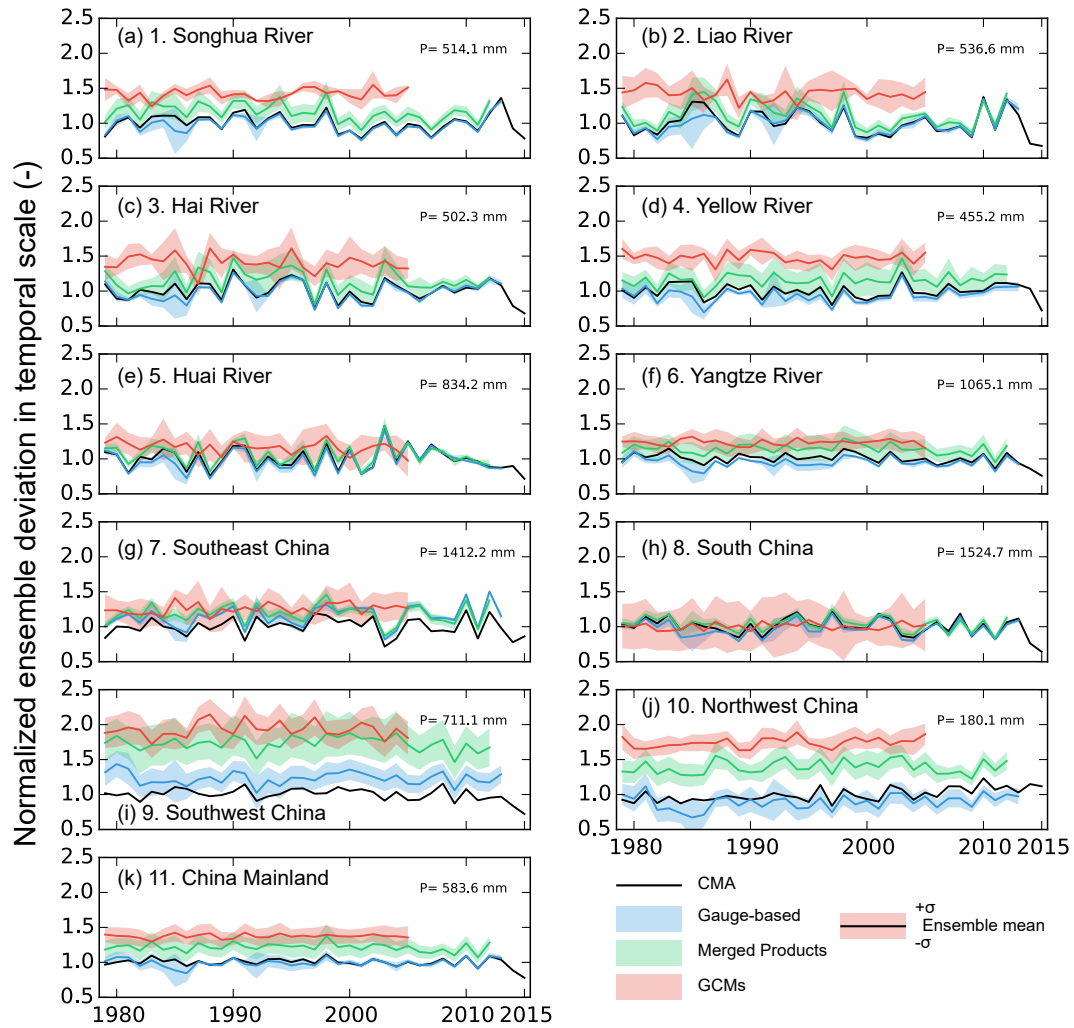
Figure 6. The temporal evolution of the model uncertainty, which is expressed as the normalized ensemble deviation of annual precipitation across datasets in each precipitation group for specific subregions. The value on the top right of each panel is the annual regional precipitation estimated in CMA dataset (1979-2015). The annual precipitation is normalized as the ratio to the CMA long-term annual precipitation. The solid curve represents the ensemble mean of precipitation in each precipitation data group over the subregion. The width of shaded area represents the standard deviation of the annual precipitation in each year among the datasets within that group (divided by the annual precipitation of the corresponding group). The shaded area distributes equally in the two sides of the ensemble mean values for the corresponding precipitation group.

The annual precipitation of the GCMs (the red curve) is apparently higher than that of the gauge-based products or merged products for almost all regions, which agrees with the spatial patterns in Figure 4-d.

The ensemble deviation (shaded area) shown in Figure 6 represents the variations of the products in the same precipitation group. The normalized deviation facilitates the comparisons between different regions. High deviations are found in all three precipitation groups in the southwestern China (Figure 6-i) because of the large differences along the Himalayas. The deviations among the gauge-based products and the merged products in other regions are small and getting smaller with time. It is mainly because more observations are integrated and technologies improve with time to control the data quality. A large deviation is found in the merged products in 10-northwest China (Figure 6-j) and the 4-Yellow River Basin (Figure 6-d), where the annual precipitation is among the lowest and dry climate dominates. The model deviation of GCMs varies among regions as it is smallest in the 1-Songhua River Basin (Figure 6-a) and the 6-Yangtze River Basin (Figure 6-f), while it is among the highest in the 8-south China and the west China (9,10), agreeing with the deviation maps in Figure 5.

Despite of the difference in mean values, the temporal evolution of the gauge-based products and merged products agree well with that of the CMA dataset, while the temporal evolution of GCMs ensemble is weaker and not well correlated with that of the CMA. The main reason is that GCMs are not constrained in their synoptic variability and the sequence of the wet and dry years can be very different from that of the observations. So, a smoother result can be obtained when we build the ensemble means from the GCMs. While this is different for the gauge-based and merged products, as they have a strong co-variance and the ensemble mean preserves this co-variance.

For the entire mainland of China (Figure 6-k), the ensemble deviation remains stable for different precipitation groups. In contrast, the annual precipitation spans the largest spatial heterogeneity in the mainland compared to those divided subregions (Figure 4). However, the spatial variation has been collapsed when estimating the regional precipitation for temporal analysis. It is therefore interesting to see how the uncertainty estimate changes when the variations in the time dimension and in the space dimension are considered together in the precipitation datasets.

3.4 Variations in the time and space dimensions

The precipitation varies in time and space; however, it is averaged either in the time dimension to obtain the spatial patterns of model uncertainty (Figure 5) or in the space dimension to obtain the temporal evolution of the model uncertainty (Figure 6). But the deviations in the time and space dimensions are indeed very rarely compared. Herein, the standard deviation of the temporal and spatial variations in the precipitation datasets are compared in Figure 7 in ten subregions and the Chinese mainland for different precipitation groups.

The gauge-based products provide similar annual regional precipitation to CMA over the China mainland and ten specific regions except for the region 7-southeast China (Figure 7-g) and region 9-southwest China (7-i). While the merged products show larger precipitation estimations for most of the regions. It might indicate the degraded ability of remote sensing, the important data source in the merged products, to estimate the precipitation amount in storms as the storms mainly contribute to the total precipitation for the two subregions. The regional precipitation is larger in merged products than that of observations

and the magnitude of the deviation in GCMs is even larger except in the region 8-south China (Figure 7-h). These results indicate the degraded ability of merged products and GCMs in reproducing the total value of the annual precipitation.
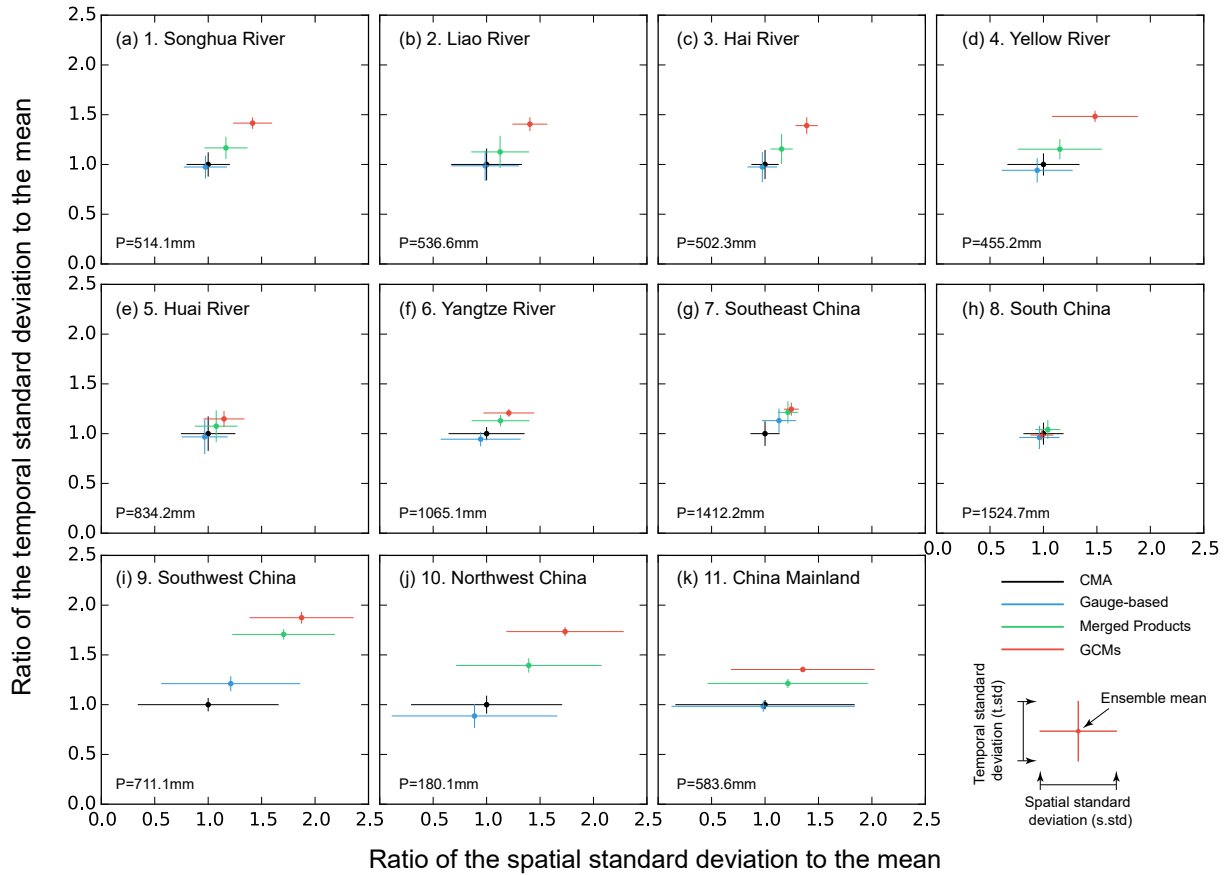
Figure 7. The spatial standard deviation (horizontal) and temporal standard deviation (vertical) of the annual precipitation in different precipitation groups for ten regions and the mainland China. The cross center represents the long-term means of the regional annual precipitation. The horizontal error bar represents the spatial standard deviation (spatial variation of the long-term annual precipitation at all the grids). The vertical error bar represents the temporal standard deviation (temporal variations of region-averaged annual precipitation in different years). The P values in the left bottom is the annual precipitation of CMA.

Regarding the variations in time and space dimensions, the regions 9, 10 and 11 have the largest ratio of the spatial standard deviation (to the mean), indicating the most significant spatial heterogeneity over the regions. The 7-southeast and the 3-Hai River have the smallest variations either because of the small area or because of the homogeneity in the subregion as the spatial correlation is high in the area. The relative ratio of the temporal standard deviation to the spatial standard deviation is among the smallest in the regions 9, 10 and 11 (k=0.1, 0.12 and 0.05, respectively. k is the ratio of the temporal deviation to the spatial deviation), showing an apparent difference between the variation in the time and space dimensions. While, the

difference between variation in two dimensions is small in the 3-Hai River basin (k=1.15) and 7-southeast China (k=0.90), mainly because the relatively strong variability of the annual precipitation in different years.

In addition to the differences across regions, the variations in different precipitation groups also vary in magnitude. Excluding the CMA dataset which only consists of one single product, the total variation (sum of the spatial and temporal variation) in the gauge-based products are higher than that of the other two groups. The difference demonstrates that on one hand the gauge-based may have the largest variation over space or on the other hand the correlation among different gauge-based products are high so that the variation is preserved when doing the ensemble. On the contrary, the GCMs have the smallest variations, either because the precipitation estimated in GCMs are more homogenous over space, or because the spatial patterns in different GCMs are not consistent and the spatial correlation is lower since there is no constrain in the GCM simulation.

4 Variances in precipitation products

4.1 Variances in three dimensions

We have introduced the general spatial and temporal characteristics of the precipitation in different groups and their variations in different dimensions in the above section. In this section, we will present the results that estimated by the newly proposed variance approach. As introduced in the methodology section, the input annual precipitation to the approach is re-organized into three dimensions as (1) **time**, 27 years from 1979 to 2005, (2) **space**, the number of 0.5º grids in a specific region and (3) **ensemble**, the number of the models in a same precipitation group (four models in all three groups).

The grand variance and its three components (i.e., variance in time, space and ensemble dimension) for all the subregions are mapped in Figure 8. The grand variance (total value of the variance for all three dimensions) is similar for data groups of gauge-based products and the merged products (Figure 8-a,b,c), while the grand variance in GCMs is large and is approximating twice the values of the other two groups in regions 9-south China and 10-southwest China. The differences are mainly constituted by the space variance and ensemble variance (Figure 8-i,l).

The time variance (V_t) is the smallest among all three variance proportions, and there are very little differences of V_t in the northern China (Figure 8-d,e,f). V_t in the gauge-based products is higher than that in the merged products and GCMs in regions 8-southeast China and 9-south China, indicating a relatively strong temporal variation in the annual precipitation series which consists with the larger uncertainty ranges shown in Figure 6-h,i. Similar patterns of the space variance (V_s) are found in the gauge-based products and merged products (Figure 8-g,h). The 7-Yangtze River basin and 9-southwest China have the largest V_s because the precipitation significantly varies in space in these two regions. V_s is higher in the precipitation of GCMs especially in the 9-southwest China, indicating the strong spatial heterogeneity in the GCM models over the Himalayas (Figure 8-i). The ensemble variance (V_e) is relatively small in most regions in gauge-based products (Figure 8-j), with the highest V_e occurring in 9-southwest China. It indicates that the model variation between datasets in the observation group is small. Similar small values of V_e are found in the northern regions in merged products as well as in the GCMs for the regions in the northern China, while the intra-ensemble variations are large in the south especially the 9-southwest China and 8-south China in the GCMs (Figure 8-k,l).
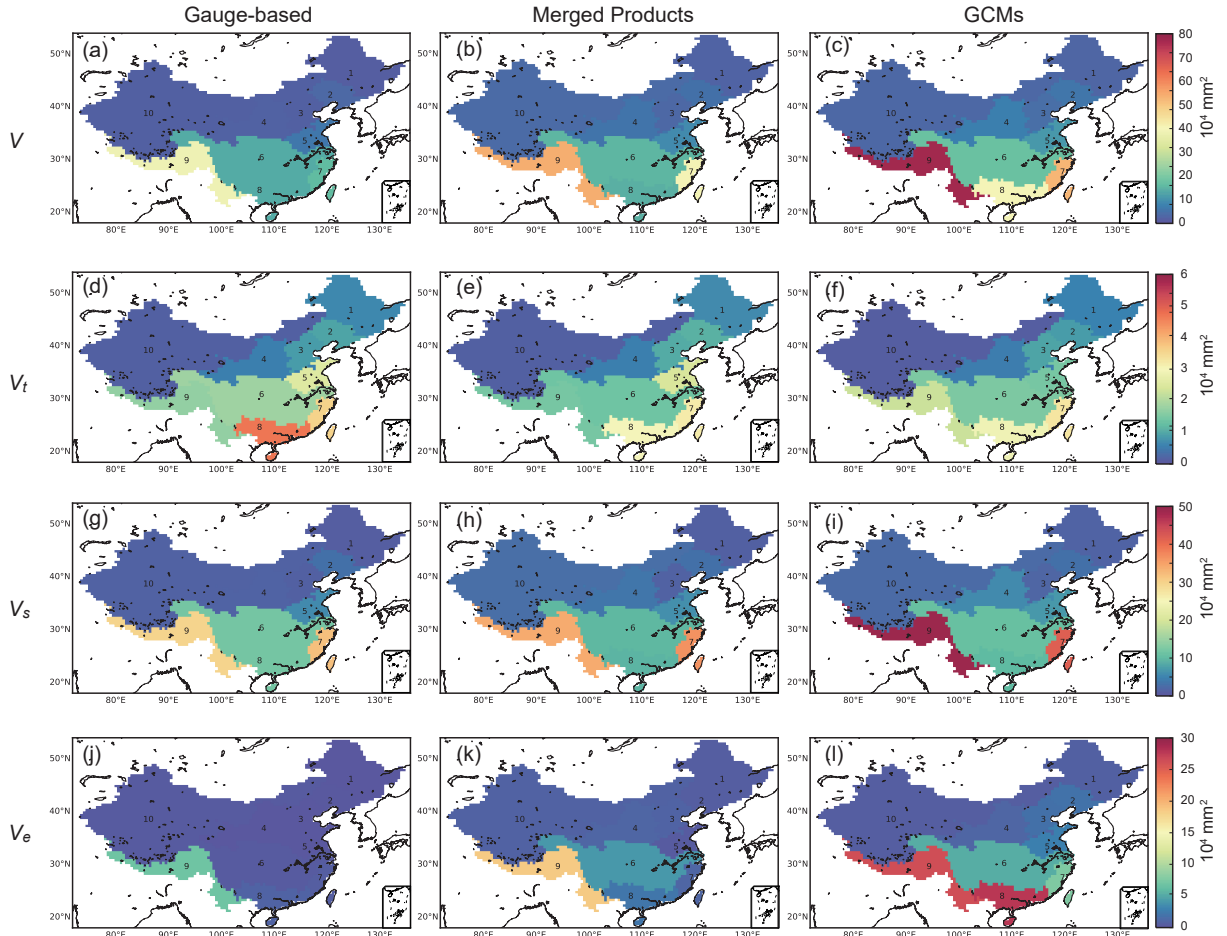
Figure 8. The maps of the grand variance (V) and variances in different dimensions (V_t, V_s, V_e) for three different precipitation groups.

In conclusion, the grand variance and individual variance for each of the three different dimensions are generally larger in the dataset group consisting of GCMs. The variations for the gauge-based products and merged products are similar in values and spatial distribution. However, in addition to the variances, the uncertainty defined as the ratio of the square root of the variance to the mean (i.e., U, U_t, U_s, U_e) contains extra information of the regional means, and will be discussed in the following section.

4.2 Deviations in three dimensions

In contrast to the spatial patterns of the variance magnitude distributed in the ten subregions (Figure 8), the larger values of the deviation ($U = \sqrt{V}/\mu$) occur in the northwest, and lower values occur in the southern China in general (Figure 9). A possible reason is the decreasing tendency of precipitation magnitude from the southeast to the northwest (Figure 4). Although the variances are among the lowest in the northwest China, the total deviation is the highest in this region (U=0.89, Figure 9-a,b,c)

for all three precipitation groups because of the low precipitation rate in the northwest. U is relatively small in the 1-Songhua River (U=0.27) in the northeast and 8-South China (U=0.29) for the gauge-based products and 6-Yangtze River has relatively lower U in the merged products and GCMs in the east part of China.
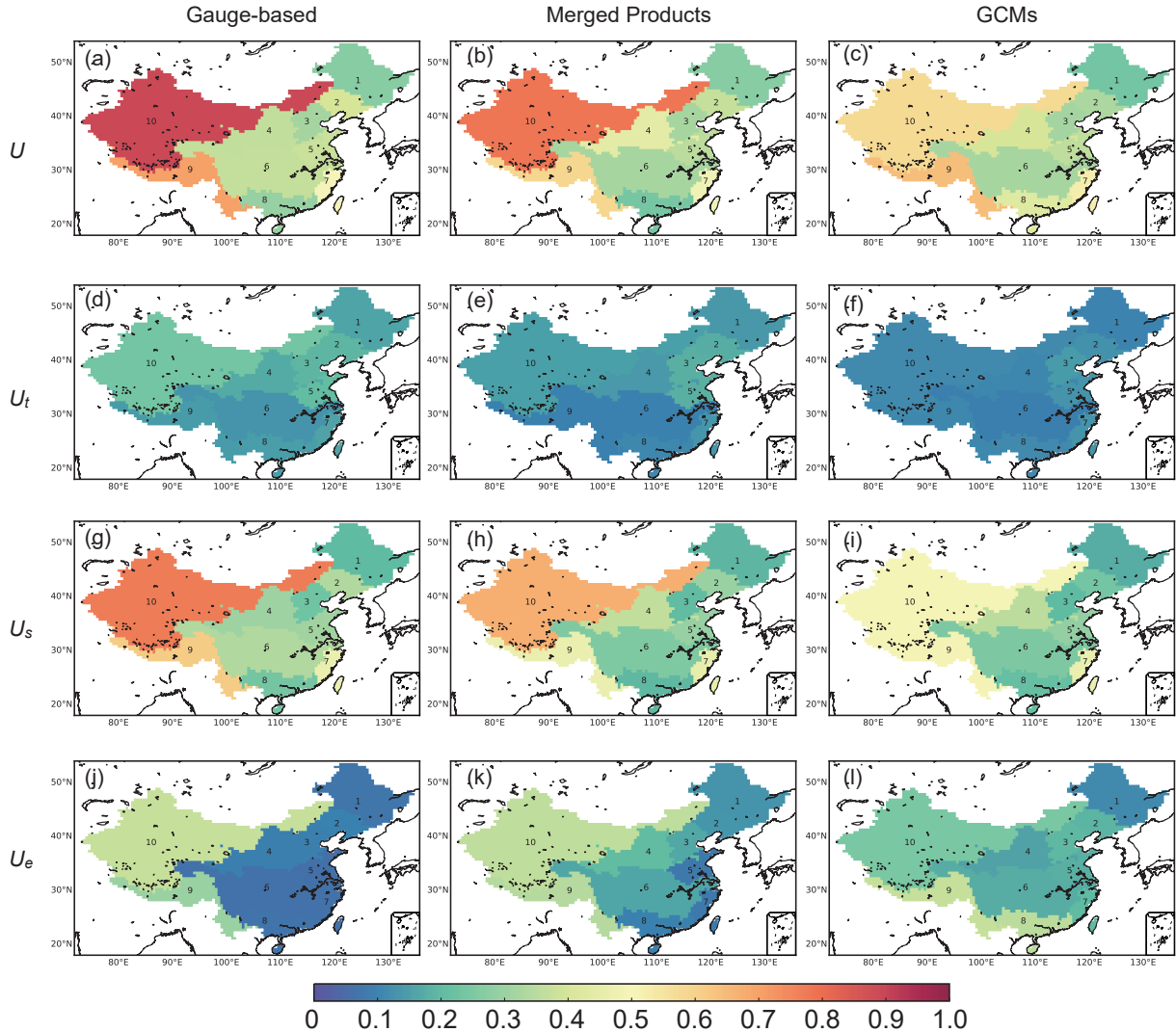
Figure 9. The maps of deviations (U, U_t, U_s, U_e) estimated as the ratio of the square root of the corresponding variances (i.e., V, V_t, V_s, V_e) to the regional mean (μ) for three different precipitation groups. Among which, the U_e is considered as the model uncertainty.

The variations in time and space dimension are inherent, and they show the temporal evolution and spatial heterogeneity of the characteristics in different precipitation products. It is found that the U_t is small and contributes very little to the total U, indicating the weak fluctuation of annual precipitation compared to spatial variations (Figure 9-d,e,f). The smallest U_t value for the GCMs is in accordance with the weakest temporal variations in Figure 6. The relative variance in space dimension (U_s)

contributes the most to the total variance, especially in the northwestern China (U_s=0.77 for the gauge-based products, Figure 9-g). The high values indicate the strong spatial heterogeneity of precipitation in the region compared to the mean values. It indicates that the ability to describe the precipitation significant varies in different places in the subregions. However, because the spatial variations characterized by GCMs in the northwestern China is less significant than other two groups, the U_s for region 10-southwest China (=0.51) is smaller than that of the gauge-based and merged products.

The variations in time and space dimensions show the natural precipitation patterns but the deviation of the values at same spatiotemporal points show the ability of the products to consistently represent the spatiotemporal patterns. The relative variance in the ensemble dimension (U_e) shows the variations among different products in the same group. For the gauge-based products, the U_e is smaller than 0.1 for regions in the eastern China, indicating that the model differences are relatively small compared to the annual means. The U_e value is higher for the 9-southwest (=0.30) and 10-northwest China (=0.37), showing large variations even in the gauge-based products. For the merged products, U_e is similar to that of the gauge-based products in the western China (=0.36), while it is larger in the east especially for the 6-Yangtze River and 4-Yellow River (more than two times larger than U_e of the gauge-based products).

For the GCM precipitation, the uncertainty increases compared to the other two groups in the eastern regions, corresponding to the higher ensemble variations in GCM over the eastern regions shown in Figure 5. While, it decreases in 10-northwest China (U_e=0.25) and a possible reason is that the spatial homogeneity of the variations in the region 10-northwest China (Figure 5-f) is stronger than that of the other groups (Figure 5-b,d). In the GCMs, the highest U_e occurs in the southwestern China where both the means and the variations are higher (Figure 4 and 5). In conclusion, the U_e is linked with the magnitude of the model uncertainties in Figure 5 and Figure 6. It indicates that the U_e is to some degree correlated to the classic metrics as the higher U_e covers the grid cells or regions with higher model uncertainty.

5 Uncertainty and metrics comparison

5.1 Deviation from the classic uncertainty metrics

The new estimates of the uncertainty U_e provide a comprehensive evaluation of the uncertainty over space and time, and the values are affected by both the temporal variation and the spatial homogeneity (spatial correlations) among the different examined products. In this section, we will compare the uncertainty (U_e) estimated by the three-dimensional partitioning approach with the two classic metrics (defined as $N.s.std$ in Eq. 28 and $N.t.std$ in Eq.29), to explain how these three metrics are related and differ with each other.

As shown in Figure 10, U_e is correlated to both the $N.s.std$ and $N.t.std$, especially when U_e is smaller than 0.2 where the regions from 1 to 8 are generally included for all three precipitation groups. The U_e is in general larger than the $N.s.std$ and $N.t.std$ for the products. And the deviation is because the variations of the other dimension have collapsed when calculating the spatial deviation (or temporal deviation). For the regions 9, 10 and 11, the values of the $N.s.std$ and $N.t.std$ deviate the most from the 1:1 line of the U_e. Taking subregion 9-southwest China in the gauge-based products as an example, the temporal variance is 62.4 mm yr^{-1} while the spatial variance is 571.8 mm yr^{-1} (Figure 7-i). The difference between $N.s.std$ and
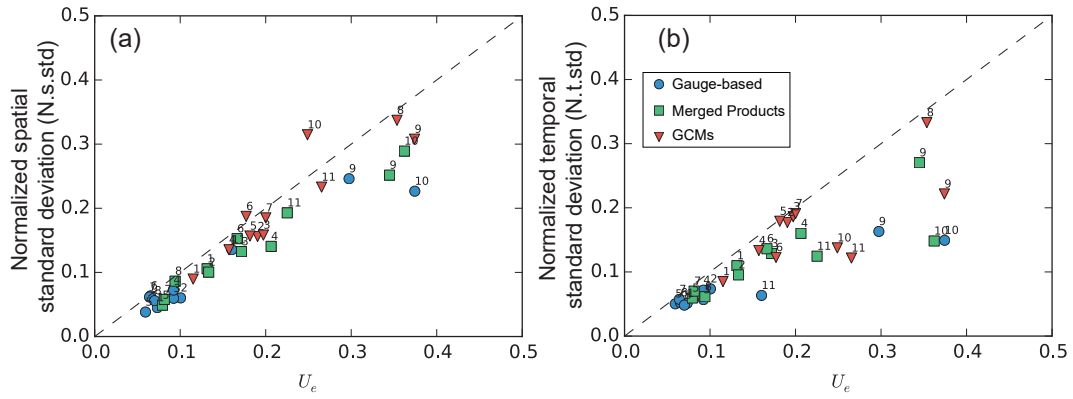
Figure 10. The relation of the U_e to two classic metrics as (a) the normalized spatial standard deviation - $N.s.std$ and (b) the normalized temporal standard deviation - $N.t.std$.

U_e is 0.058 (=0.297-0.239, changing ratio is 24.3%) when the temporal variation is collapsed while the difference between $N.t.std$ and U_e is 0.126 (=0.297-0.171, changing ratio is 73.4%) when the spatial variation, which is significantly larger than the temporal variation, is collapsed.

These regions (9, 10, 11) feature strong spatial heterogeneities (Figure 7-i,j,k) in the annual mean precipitation (Figure 4).

5   The spatial correlation of the annual precipitation and the temporal correlation of the regional precipitation is also weaker in these three regions than other regions (*not shown in the results*). The averaging process before estimating classical metrics will cause a significant smooth of the datasets when the spatial correlation among datasets are very low. The spatial variation across space is also significantly higher than temporal variations (Figure 7). Because the estimation of $N.t.std$ needs the averaging in spatial dimension which may include more information than that in the time dimension, the deviation between $N.t.std$ and

10   U_e (Figure 10-b) is larger than that between $N.s.std$ and U_e (Figure 10-a). The priority of the precipitation types also changes from the model dominated (the model uncertainty in GCMs are larger than the other) to the region dominated (uncertainty in specific regions 9,10,11 are larger than other regions no matter in which precipitation data). This indicates that difference of model uncertainty over space has been reflected in the new uncertainty U_e.

Each classical metric has its physical meanings as the $N.s.std$ represents the uncertainties across space and $N.t.std$ repre-

15   sents the uncertainties across time. The comparison of U_e with each of them demonstrates the metric performance on the same physical meaning. It is possible to compare U_e with a combination of the two classical metrics, but the combination can be far more complex than a simple sum. However, the qualitative comparison is accessible because U_e has a linear correlation with either of them. The correlation will also remain between U_e and a combination of the two classic metrics by summing up them with certain weights.

5.2 Decomposition of the ensemble uncertainty

We now decompose the ensemble variance to explore the possible reason for the deviation of U_e from the $N.s.std$ and $N.t.std$. As shown in Eq. (26), the ensemble variance (V_e) is formulated as

$$V_e = \frac{1}{3}\left[\frac{\overline{\sigma^2_{e\_t}} + \overline{\sigma^2_{e\_s}}}{2} + \overline{\sigma^2_e} + \sigma^2_e(\mu_{ts})\right] \tag{30}$$

5   It combines four components which stand for the variation of different estimates across the ensemble dimension (i.e., the variance of original temporal and spatial values - $\overline{\sigma^2_e}$, of the temporal mean - $\overline{\sigma^2_{e\_t}}$, of the spatial mean - $\overline{\sigma^2_{e\_s}}$ and of the grand mean - $\sigma^2_e(\mu_{ts})$). Among which, the $\overline{\sigma^2_{e\_t}}$ is the mean of the square of spatial standard deviation in Figure 5-a,c,e for all grids in a specific region and $\overline{\sigma^2_{e\_s}}$ is the mean of the square of the temporal standard deviation in Figure 6 for each time step in a specific region. These two components are related to the two classic metrics $N.s.std$ (Eq. 28) and $N.t.std$ (Eq. 29), respectively.
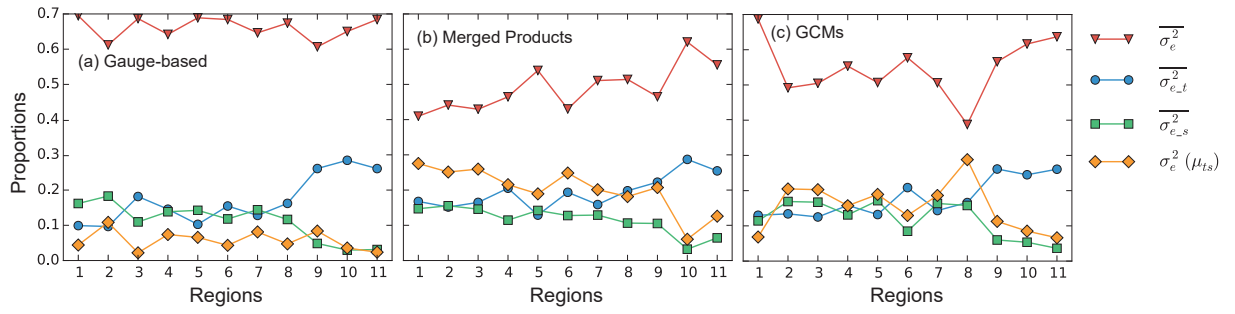
Figure 11. The proportion of the four components in Eq. (30) to the V_e in three precipitation groups, (a) gauge-based products, (b) merged products and (c) GCMs. The contribution is normalized so that the sum of them is 1.0 for each region. Among the four components, the $\overline{\sigma^2_{e\_t}}$ and $\overline{\sigma^2_{e\_s}}$ are associated with the two classic metric $N.s.std$ and $N.t.std$, respectively.

10   By decomposing the Eq. (30), the contributions of the four components to the ensemble variance (V_e) are shown in Figure 11. For all three precipitation groups, $\overline{\sigma^2_e}$ is the dominant component simply because all the information on variations among the original datasets is retained in the uncertainty estimation. While, the other three components are estimations after averaging is performed in time, space or the full spatiotemporal dimensions, which indicates a loss of information. The contribution of the $\overline{\sigma^2_{e\_t}}$ and $\overline{\sigma^2_{e\_s}}$ is approximating 0.15 for regions from 1 to 8. While the $\overline{\sigma^2_{e\_t}}$ increases for the region 9, 10 and 11, indicating

15   that the spatial heterogeneity is significant for these regions. On the contrary, $\overline{\sigma^2_{e\_s}}$ decreases because the spatial averaging has collapsed the spatial variations. The very small contribution of $\overline{\sigma^2_{e\_s}}$ related to $N.t.std$ is the cause for larger deviations between $N.t.std$ and U_e (Figure 10-b).

Although all the components can be used as metrics for evaluating the variations among multiple datasets, there are limitations for each of the variations. For the variation of temporal mean $\overline{\sigma^2_{e\_t}}$ and spatial mean $\overline{\sigma^2_{e\_s}}$, the collapse of a dimension has

20   ignored part of the information (also introduced in the Introduction). Moreover, the variation of the grand mean $\sigma^2_e(\mu_{ts})$ has ignored both the temporal variability and spatial heterogeneity, which further decreases its applicability in uncertainty assess-

ment. The variation $\overline{\sigma_e^2}$ is estimated based on the original data without averaging, and thus it represents the most information. However, it cannot account for the systematic uncertainty (bias in the mean values) which is expressed as $\sigma_e^2(\mu_{ts})$.

    Therefore, all the four components represent the model variations from different aspects and neither of the single component is able to represent all the others. Integration of different components (V_e) is therefore a solution to indicate all metrics to
5   different degrees. What is interesting is that the variability of the proportions of $\overline{\sigma_{e\_t}^2}$ and $\overline{\sigma_{e\_s}^2}$ (or $\overline{\sigma_e^2}$ and $\sigma_e^2(\mu_{ts})$) are opposite and the sum of their proportions is stable around 0.3 (or 0.7). This indicates a complementary relation between the two pairs of elements ($\overline{\sigma_{e\_t}^2}$ & $\overline{\sigma_{e\_s}^2}$; $\overline{\sigma_e^2}$ & $\sigma_e^2(\mu_{ts})$). On the other word, some of the information is ignored in one of the components but remained in the other one within the same pair. And therefore, it indicates that the variation in the time dimension and that in the space dimension should be considered together as done in the estimation of the ensemble variance (V_e). The normalized
10 metric (U_e) derived from the integrated variation (V_e), which has better ability to demonstrate the uncertainties compared to the classic metrics, should be a properer choice for the uncertainty analysis.

5.3   Metrics differences in value and proportion

Figure 10 shows that the U_e is generally higher than the uncertainty identified by the two classic metrics. $N.s.std$ and $N.t.std$. Figure 12 then summaries the magnitude of the changes from the classic metrics to the new uncertainty identified by U_e. We
15 can find that the two classic metrics generally underestimate the uncertainty by around 0.03 (Figure 12-a). The variation of the underestimation of $N.t.std$ is larger than that of the $N.s.std$, showing a larger deviation between the U_e with $N.t.std$. Applying the new uncertainty metric will increase the estimation of uncertainty by around 20-40% for half of the cases compared to the $N.s.std$ (Figure 12-b). For nearly 25% of the cases, the new U_e increases the estimation of uncertainty by more than 50%. In the extreme cases, U_e is larger than twice $N.t.std$ (Figure 12-b). The results show that the known uncertainty estimated
20 by the two classic metrics, which have been widely applied to climatic analysis, have underestimated the uncertainty among different models / datasets. The underestimation may especially occur for assessment of temporal evolution of the uncertainties ($N.t.std$), which is very commonly seen in scientific reports and articles to illustrate the temporal evolution of the variables of interest.

6   Discussion and Conclusion

25 ### 6.1   Features and applicability of the approach

The total variation of the database which consists of multiple datasets is contributed by the spatio-temporal variations as well as the uncertainties among the datasets. While the uncertainty assessment with current approaches (e.g., eqs. 28 and 29) needs either the temporal variation or the spatial heterogeneity to be averaged which means a loss of information and bias in uncertainty estimation. The proposed variance partitioning approach in this study works in three dimensions. It uses
30 all the information across the time and the space dimensions among the multiple ensemble members, thus it provides a more accurate uncertainty estimation. The proposed U_e is especially suitable for the overall assessment among multiple datasets over
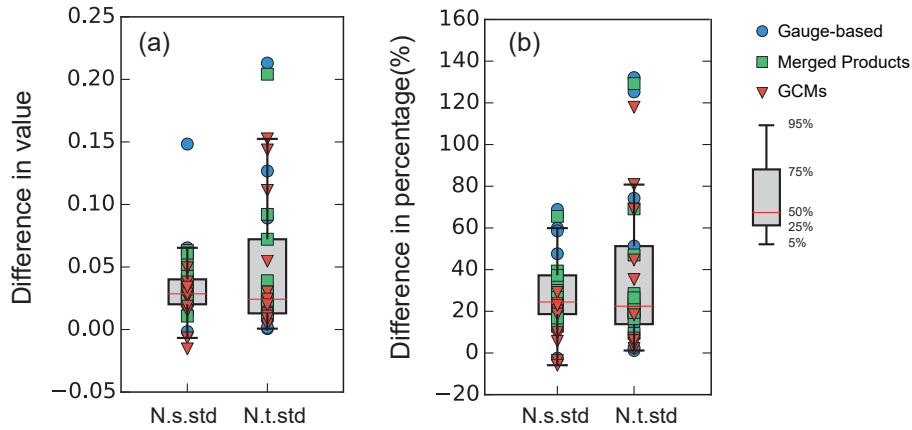
Figure 12. The changes in (a) value and (b) percentage when using U_e as the new uncertainty metric compared to classic metrics $N.s.std$ (Eq. 28) and $N.t.std$ (Eq. 29).

a certain period and over a specific space. Though, the compensation is that the U_e cannot provide the temporal evolution or spatial heterogeneity for users' consideration. In many cases we would like to know the general performance of the ensemble models with a single estimate.

The results of the partitioning approach can be affected by the choice of the time step intervals. For example, the time
5   variation or time variance proportion will significantly increase if the time interval is chosen as one month. The inter-annual variation of precipitation will result in higher V_t and lower V_s or V_e. It depends how significant the inter-annual variability is compared to the intra-annual variations. Moreover, changes in the temporal variation (increase or reduce the variation magnitude while remain the average values) will be captured in the U_e while $N.s.std$ will keep the same because the temporal variation has been neglected in the averaging process. The case will be the same for $N.t.std$.
10   The proposed approach has a flexible structure that potentially deals with different problems from global to regional dimensions. The time dimension can consider intervals from daily, monthly, annual or to decadal analysis in different scopes. The ensemble dimension is applicable from 2 members (i.e., model evaluation between simulations and observations) to any number of multi-models (consensus evaluation, Tebaldi et al., 2011; McSweeney and Jones, 2013). The present approach is applicable to any variables that are organized in the three dimensions such as climatic variables (e.g., temperature, evaporation),
15   hydrological variables (e.g., soil moisture, runoff) or environmental variables (e.g., drought index). Based on these advantages, the three-dimensional partitioning approach can widely be applied in the hydro-climatic analysis.

6.2 Conclusion

A new three-dimensional partitioning approach is proposed in this study to assess the model uncertainties among multiple datasets. The new uncertainty metric (U_e) is estimated with an overall consideration of temporal and spatial variations among
20   the ensemble products. Results show that U_e is generally larger than the classical uncertainty metrics $N.s.std$ and $N.t.std$

which require a collapse in either of the time or space dimension. The deviation occurs where the spatial variations are significant but being averaged in $N.t.std$ estimation. The decomposing of the V_e shows the complementary relation of the two classic metrics and therefore the new uncertainty U_e (derived from V_e) is a more comprehensive estimation of uncertainty.

Thirteen precipitation datasets generated by different methodologies are categorized into three groups (i.e., gauge-based products, merged products and GCMs) and the model uncertainty in the ensemble products in the same group is analyzed with the new and two classic uncertainty metrics. The GCMs are identified with the largest model uncertainty with the classical metrics in most regions, while the new estimation U_e indicates the largest model uncertainty occurs in specific regions no matter in which precipitation group. The spatial heterogeneity of the model uncertainty over space has been represented well in the new uncertainty metric. Thus, the overall model uncertainty (U_e) is a new uncertainty estimate which involves more information and should receive more attention in the uncertainty assessment field.

Appendix A: The algorithms for different expressions in the methodology

Zone A:

A1: $\mu_t[s, e; n \times l]; \mu_t[j, k] = \frac{1}{m} \sum_{i=1}^{l} z_{ijk}$

A2: $\mu_s[e, t; l \times m]; \mu_s[k, i] = \frac{1}{n} \sum_{j=1}^{l} z_{ijk}$

A3: $\mu_e[t, s; m \times n]; \mu_e[i, j] = \frac{1}{l} \sum_{k=1}^{l} z_{ijk}$

Zone B:

B1: $\sigma_t^2[s, e; n \times l]; \sigma_t^2[j, k] = \frac{1}{m} \sum_{i=1}^{l} (z_{ijk} - \mu_t[j, k])^2$

B2: $\sigma_s^2[e, t; l \times m]; \sigma_s^2[k, i] = \frac{1}{n} \sum_{j=1}^{l} (z_{ijk} - \mu_s[k, i])^2$

B3: $\sigma_e^2[t, s; m \times n]; \sigma_e^2[i, j] = \frac{1}{l} \sum_{k=1}^{l} (z_{ijk} - \mu_e[i, j])^2$

Zone C:

C1: $\sigma_{t\_s}^2[e; l]; \sigma_{t\_s}^2[k] = \sigma^2(\mu_s[k, :])$

C2: $\sigma_{t\_e}^2[s; n]; \sigma_{t\_e}^2[j] = \sigma^2(\mu_e[:, j])$

C3: $\sigma_{s\_t}^2[e; l]; \sigma_{s\_t}^2[k] = \sigma^2(\mu_t[:, k])$

C4: $\sigma_{s\_e}^2[t; m]; \sigma_{s\_e}^2[i] = \sigma^2(\mu_e[i, :])$

C5: $\sigma_{e\_t}^2[s; n]; \sigma_{e\_t}^2[j] = \sigma^2(\mu_t[j, :])$

C6: $\sigma_{e\_s}^2[t; m]; \sigma_{e\_s}^2[i] = \sigma^2(\mu_s[:, i])$

Zone D:

D1: $\mu_{et}[s; n]; \mu_{et}[j] = \frac{1}{lm} \sum_{k=1}^{l} \sum_{i=1}^{m} z_{ijk}$

D2: $\mu_{se}[t; m]; \mu_{se}[i] = \frac{1}{nl} \sum_{j=1}^{n} \sum_{k=1}^{l} z_{ijk}$

D3: $\mu_{ts}[e; k]; \mu_{ts}[k] = \frac{1}{mn} \sum_{i=1}^{m} \sum_{j=1}^{n} z_{ijk}$

Zone E:

E1: $\sigma_{et}^2[s; n]; \sigma_{et}^2[j] = \frac{1}{lm} \sum_{k=1}^{l} \sum_{i=1}^{m} (z_{ijk} - \mu_{et}[j])^2$

E2: $\sigma_{se}^2[t;m]; \sigma_{se}^2[i] = \frac{1}{nl}\sum_{j=1}^{n}\sum_{k=1}^{l}(z_{ijk} - \mu_{se}[i])^2$

E3: $\sigma_{ts}^2[e;l]; \sigma_{st}^2[k] = \frac{1}{mn}\sum_{i=1}^{m}\sum_{j=1}^{n}(z_{ijk} - \mu_{ts}[k])^2$

Zone F:

F1: $\sigma_t^2(\mu_{se}) = \frac{1}{m}\sum_{i=1}^{m}(\frac{1}{nl}\sum_{j=1}^{n}\sum_{k=1}^{l}z_{ijk} - \frac{1}{m}\sum_{i=1}^{m}(\frac{1}{nl}\sum_{j=1}^{n}\sum_{k=1}^{l}z_{ijk}))^2$

5 F2: $\sigma_s^2(\mu_{et}) = \frac{1}{n}\sum_{j=1}^{n}(\frac{1}{lm}\sum_{k=1}^{l}\sum_{i=1}^{m}z_{ijk} - \frac{1}{n}\sum_{j=1}^{n}(\frac{1}{lm}\sum_{k=1}^{l}\sum_{i=1}^{m}z_{ijk}))^2$

F3: $\sigma_e^2(\mu_{ts}) = \frac{1}{l}\sum_{k=1}^{l}(\frac{1}{mn}\sum_{i=1}^{m}\sum_{j=1}^{n}z_{ijk} - \frac{1}{l}\sum_{k=1}^{l}(\frac{1}{mn}\sum_{i=1}^{m}\sum_{j=1}^{n}z_{ijk}))^2$

The t, s, e in the algorithms represents the three dimensions **time**, **space** and **ensemble**, with the size of m, n, l, respectively. Each expression is shown with its size and the meaning of each dimension. For example, for the A1: $\mu_t[s,e;n \times l]$, the μ_t has a size of $n \times l$. The first axis represents the space dimension, and the second is the ensemble dimension. While C1 ($\sigma_{t\_s}^2[e;l]$)

10 has only one ensemble dimension with its size as l. F1 ($\sigma_t^2(\mu_{se})$) is only a single value.

Author contributions. XZ initialized the ideas presented in this paper with supervising from JP and TY. XZ prepared the simulations, the figures and the manuscript. CSH participated in the data preparation. All authors contributed to the discussion and revising the paper.

Competing interests. The authors declare that they have no conflict of interest.

Acknowledgements. This study was supported by the National Natural Science Foundation of China (grant nos. 41561134016 and 51879068);

15 the CHINA-TREND-STREAM French national project (ANR grant no. ANR-15-CE01-00L1-0L); the National Key Research and Development Program (2018YFC0407900) and the China Scholarship Council (CSC, 201506710042). The work was supported by computing resource of the IPSL ClimServ cluster at École Polytechnique, France.

References

Adler, R. F., Sapiano, M. R., Huffman, G. J., Wang, J. J., Gu, G., Bolvin, D., Chiu, L., Schneider, U., Becker, A., Nelkin, E., Xie, P., Ferraro, R., and Shin, D. B.: The Global Precipitation Climatology Project (GPCP) monthly analysis (New Version 2.3) and a review of 2017 global precipitation, Atmosphere, 9, https://doi.org/10.3390/atmos9040138, https://www.esrl.noaa.gov/psd/data/gridded/data.gpcp.html, 2018.

Beck, H. E., Vergopolan, N., Pan, M., Levizzani, V., Van Dijk, A. I., Weedon, G. P., Brocca, L., Pappenberger, F., Huffman, G. J., and Wood, E. F.: Global-scale evaluation of 22 precipitation datasets using gauge observations and hydrological modeling, Hydrology and Earth System Sciences, 21, 6201–6217, https://doi.org/10.5194/hess-21-6201-2017, http://gloh2o.org, 2017.

Bosshard, T., Carambia, M., Goergen, K., Kotlarski, S., Krahe, P., Zappa, M., Schär, C., and Schar, C.: Quantifying uncertainty sources in an ensemble of hydrological climate-impact projections: UNCERTAINTY SOURCES IN CLIMATE-IMPACT PROJECTIONS, Water Resources Research, 49, 1523–1536, https://doi.org/10.1029/2011WR011533, 2013.

Dee, D. P., Uppala, S. M., Simmons, A. J., Berrisford, P., Poli, P., Kobayashi, S., Andrae, U., Balmaseda, M. A., Balsamo, G., Bauer, P., Bechtold, P., Beljaars, A. C., van de Berg, L., Bidlot, J., Bormann, N., Delsol, C., Dragani, R., Fuentes, M., Geer, A. J., Haimberger, L., Healy, S. B., Hersbach, H., Hólm, E. V., Isaksen, L., Kållberg, P., Köhler, M., Matricardi, M., Mcnally, A. P., Monge-Sanz, B. M., Morcrette, J. J., Park, B. K., Peubey, C., de Rosnay, P., Tavolato, C., Thépaut, J. N., and Vitart, F.: The ERA-Interim reanalysis: Configuration and performance of the data assimilation system, Quarterly Journal of the Royal Meteorological Society, 137, 553–597, https://doi.org/10.1002/qj.828, https://www.ecmwf.int/en/forecasts/datasets/archive-datasets/reanalysis-datasets/era-interim, 2011.

Déqué, M., Rowell, D. P., Lüthi, D., Giorgi, F., Christensen, J. H., Rockel, B., Jacob, D., Kjellström, E., De Castro, M., and Van Den Hurk, B.: An intercomparison of regional climate simulations for Europe: Assessing uncertainties in model projections, Climatic Change, 81, 53–70, https://doi.org/10.1007/s10584-006-9228-x, 2007.

Everitt, B.: The Cambridge Dictionary of Statistics, vol. 53, Cambridge University Press, https://doi.org/10.1017/CBO9781107415324.004, 2013.

Harris, I., Jones, P. D., Osborn, T. J., and Lister, D. H.: Updated high-resolution grids of monthly climatic observations - the CRU TS3.10 Dataset, International Journal of Climatology, 34, 623–642, https://doi.org/10.1002/joc.3711, 2014.

IPCC: Technical Sum- mary. In: Climate Change 2013: The Physical Science Basis. Contribution of Working Group I to the Fifth Assessment Report of the Intergovernmental Panel on Climate Change, Cambridge University Press, Cambridge, United Kingdom and New York, NY, USA, 2013a.

IPCC: Summary for Policymakers. In: Climate Change 2013: The Physical Science Basis. Contribution of Working Group I to the Fifth Assessment Report of the Intergovernmental Panel on Climate Change, Cambridge University Press, Cambridge, United Kingdom and New York, NY, USA, 2013b.

Kay, J. E., Deser, C., Phillips, A., Mai, A., Hannay, C., Strand, G., Arblaster, J. M., Bates, S. C., Danabasoglu, G., Edwards, J., Holland, M., Kushner, P., Lamarque, J. F., Lawrence, D., Lindsay, K., Middleton, A., Munoz, E., Neale, R., Oleson, K., Polvani, L., and Vertenstein, M.: The community earth system model (CESM) large ensemble project : A community resource for studying climate change in the presence of internal climate variability, Bulletin of the American Meteorological Society, 96, 1333–1349, https://doi.org/10.1175/BAMS-D-13-00255.1, 2015.

Kottek, M., Grieser, J., Beck, C., Rudolf, B., and Rubel, F.: World map of the Köppen-Geiger climate classification updated, Meteorologische Zeitschrift, 15, 259–263, https://doi.org/10.1127/0941-2948/2006/0130, 2006.

Landerer, F. W. and Swenson, S. C.: Accuracy of scaled GRACE terrestrial water storage estimates, Water Resources Research, 48, 1–11, https://doi.org/10.1029/2011WR011453, 2012.

McSweeney, C. F. and Jones, R. G.: No consensus on consensus: The challenge of finding a universal approach to measuring and mapping ensemble consistency in GCM projections, Clim. Change, 119, 617–629, https://doi.org/10.1007/s10584-013-0781-9, 2013.

5 Menne, M. J., Durre, I., Vose, R. S., Gleason, B. E., and Houston, T. G.: An overview of the global historical climatology network-daily database, Journal of Atmospheric and Oceanic Technology, 29, 897–910, https://doi.org/10.1175/JTECH-D-11-00103.1, 2012.

Phillips, T. J. and Gleckler, P. J.: Evaluation of continental precipitation in 20th century climate simulations: The utility of multimodel statistics, Water Resources Research, 42, 1–10, https://doi.org/10.1029/2005WR004313, 2006.

Rodell, M., Houser, P., Jambor, U., Gottschalck, J., Mitchell, K., Meng, C.-J., Arsenault, K., Cosgrove, B., Radarkovich, J., Bosilovich,
10 M., Entin, J., Walker, J., Lohmann, D., and Toll, D.: The Global Land Data Assimilation System, American Meteorological Society, pp. 381–394, https://doi.org/10.1175/BAMS-85-3-381, 2004.

Schewe, J., Heinke, J., Gerten, D., Haddeland, I., Arnell, N. W., Clark, D. B., Dankers, R., Eisner, S., Fekete, B. M., Colón-González, F. J., Gosling, S. N., Kim, H., Liu, X., Masaki, Y., Portmann, F. T., Satoh, Y., Stacke, T., Tang, Q., Wada, Y., Wisser, D., Albrecht, T., Frieler, K., Piontek, F., Warszawski, L., and Kabat, P.: Multimodel assessment of water scarcity under climate change, Proceedings of the National
15 Academy of Sciences, 111, 3245–3250, https://doi.org/10.1073/pnas.1222460110, 2014.

Schneider, A., Jost, A., Coulon, C., Silvestre, M., Théry, S., and Ducharne, A.: Global scale river network extraction based on high-resolution topography and constrained by lithology, climate, slope, and observed drainage density, Geophysical Research Letters, pp. 2773–2781, https://doi.org/10.1002/2016GL071844, 2017.

Sun, F., Roderick, M. L., Farquhar, G. D., Lim, W. H., Zhang, Y., Bennett, N., and Roxburgh, S. H.: Partitioning the variance between space
20 and time, Geophysical Research Letters, 37, 1–6, https://doi.org/10.1029/2010GL043323, 2010.

Sun, F., Roderick, M. L., and Farquhar, G. D.: Changes in the variability of global land precipitation, Geophysical Research Letters, 39, 1–6, https://doi.org/10.1029/2012GL053369, 2012.

Sun, Q., Miao, C., Duan, Q., Ashouri, H., Sorooshian, S., and Hsu, K. L.: A Review of Global Precipitation Data Sets: Data Sources, Estimation, and Intercomparisons, Reviews of Geophysics, 56, 79–107, https://doi.org/10.1002/2017RG000574, 2018.

25 Tapiador, F. J., Turk, F. J., Petersen, W., Hou, A. Y., Garcia-Ortega, E., Machado, L. A. T., Angelis, C. F., Salio, P., Kidd, C., Huffman, G. J., and de Castro, M.: Global precipitation measurement: Methods, datasets and applications, Atmospheric Research, 104-105, 70–97, https://doi.org/10.1016/j.atmosres.2011.10.021, 2012.

Tebaldi, C., Arblaster, J. M., and Knutti, R.: Mapping model agreement on future climate projections, Geophys. Res. Lett., 38, 1–5, https://doi.org/10.1029/2011GL049863, 2011.

30 Willmott, C. J. and Matsuura, K.: Terrestrial Air Temperature and Precipitation: Monthly and Annual Time Series (1900 - 2010), http://climate.udel.edu/data, 2012.

Xie, P., Janowiak, J. E., Arkin, P. A., Adler, R., Gruber, A., Ferraro, R., Huffman, G. J., and Curtis, S.: GPCP pentad precipitation analyses: An experimental dataset based on gauge observations and satellite estimates, Journal of Climate, 16, 2197–2214, https://doi.org/10.1175/2769.1, https://www.esrl.noaa.gov/psd/data/gridded/data.cmap.html, 2003.

35 Xie, P., Chen, M., Yang, S., Yatagai, A., Hayasaka, T., Fukushima, Y., and Liu, C.: A Gauge-Based Analysis of Daily Precipitation over East Asia, Journal of Hydrometeorology, 8, 607–626, https://doi.org/10.1175/JHM583.1, http://ftp.cpc.ncep.noaa.gov/precip/CPC_UNI_PRCP/, 2007.